[Article] Portevin-Le Chatelier effects in a high-Mn austenitic steel

PORTEVIN - LE CHATELIER EFFECTS IN A HIGH-Mn AUSTENITIC STEEL

G. Scavino, C. Di Salvo, P. Matteis, R. Sesana, D. Firrao[1]

Politecnico di Torino (Turin Technical University)

ABSTRACT

High-manganese austenitic steels were recently proposed to fabricate structural car body parts due to their very favorable combination of strength and ductility. They exhibit Portevin - Le Chatelier macroscopic plastic localization phenomena at room temperature, evidenced on the tensile curves first by isolated stress peaks corresponding to the nucleation of deformation bands, which travel along the tensile axis, and then by serrations, due to static deformation bands. The bands extend to the whole width of the specimen and cause a local temperature increase along with a slight surface relief. These plastic instabilities were studied during tensile tests at strain rates between 0.0004 and 0.04 s^{-1}, with optical video recording, infrared thermography, and optical extensometry, the latter based on digital image correlation. Two A and type C bands were observed and are described.

KEYWORDS: Portevin - Le Chatelier effect; high-Mn steels; infrared thermography; optical extensometry; digital image correlation.

[1] Fellow of ASM International

1. INTRODUCTION

High-Mn austenitic sheet steels offer a remarkable combination of strength and ductility, with ultimate tensile strengths larger than 1100 MPa and elongations-to-fracture larger than 50 % [1], which makes them strong candidates for car body applications for weight reduction. In fact, car body steels, in addition to showing high tensile strength, must also display high biaxial ductility, to allow the deep drawing of complex shapes, as well as the capability to absorb great quantities of energy during a crash to ensure the vehicle safety.

Much work has already been published on alloy development, microstructure analysis, and mechanical properties of these steels [1-9]. In particular, it was ascertained that they exhibit plastic deformation not only by dislocation slip but also by mechanical twinning [7], with the newly formed twin boundaries acting as obstacles to dislocation movement in the same way as grain boundaries do [1]. For this reason these steels are referred to as TWIP (Twinning Induced Plasticity) steels.

These steels also exhibit the Portevin - Le Chatelier (PLC) macroscopic plastic localization phenomena when subjected to tensile tests at room temperature [10-14]; these latter phenomena have been attributed either to plain dynamic strain aging due to interactions between mobile dislocations and point-defect complexes including interstitial C atoms [13], or to more complex microscopic interactions also involving twinning phenomena, not yet completely clarified [14].

In general, the PLC effect is revealed, on flat tensile specimens, by the appearance of localized deformation bands across the whole specimen width. Three types of bands can be distinguished as follows: (i) type A bands, which propagate continuously along the tensile axis; (ii) type B bands, which exhibit an intermittent propagation; and (iii) type C bands, which do not propagate. The nucleation of new PLC bands is associated with irregularities of the tensile stress-strain curve, such as serrations or local variations of stress value [15].

The localized PLC deformation phenomena, observed in a high-Mn steel, are hereafter examined by using two non-destructive, non-contact, wide-field measurement systems, namely infrared

thermography and optical extensometry. In particular, since all strain mechanisms are associated with thermal effects, the measurement of pointwise temperatures on the sample surface during the tensile tests can effectively help in the observation of the test progress. Thermographic methods have already been used for the evaluation of deformation phenomena, both plastic and elastic [9-11], which are generally associated with temperature variations in the 0.1 to 10 K temperature range.

Whereas both infrared thermography and optical extensometry have already been applied separately to study PLC phenomena in TWIP steels, [10,11,13,14,16] the present work will aim to compare and integrate the two methods for the same alloy and tensile test conditions.

2. EXPERIMENTAL PROCEDURE

2.1. Material and tensile testing

The examined steel was fabricated in the form of 1.5 mm thick sheets. Its overall chemical, crystallographic, microstructural and tensile properties were previously investigated [12], and are summarized here.

The chemical composition of the steel was (wt. %): C 0.5, Mn 22.4, Mo 0.7, V 0.22, Si 0.16, Cr 0.13, P 0.025, S < 0.001. The as-fabricated steel sheet showed homogeneous and isotropic austenite grains, with an average grain size of 3 μm, and with elemental segregation bands in the rolling directions (uncorrelated with the grains). Although the formation of equilibrium carbides was probably inhibited by the thermo-mechanical production process, small amounts of sub-micron alloy carbides, e.g. VC, may be present and may have contributed to the grain refining, together with the thermo-mechanical process itself. The deformed specimens revealed a modification of the crystallographic texture, but no new phases.

The steel tensile curves and mean tensile properties are shown in Fig. 1 and in Table I, respectively, as a function of strain rate. The TWIP steel exhibits a remarkable combination of strength and ductility, with a high and nearly constant (for each curve) strain hardening slope. By increasing the

strain rate from 0.0004 to 0.3 s^{-1}, the strain hardening slope, the ultimate tensile strength and the total elongation decrease slightly, whereas the yield strength does not vary significantly and is close to 550 MPa (Table I and Fig. 1).

The stress-strain curves show local stress peaks and serrations, as a function of the strain rate. These irregularities are associated with PLC plastic localization effects, which are also evidenced on previously polished specimens by macroscopic surface relief lines, either transient, due to A bands, or permanent, due to C bands. By increasing the strain rate from 0.0004 to 0.04 s^{-1}, the critical engineering strain value, at which the A bands start, increases from 0.17 to 0.44; and finally, at a strain rate of 0.3 s^{-1}, PLC effects are no longer detected. The A and C bands occur in separated time (or strain) intervals: the former appear first at the above mentioned critical strain values and are active for most of the remaining test duration, whereas the C bands only appear in a much shorter time interval at end of test. Both A and C bands are inclined with respect to the specimen axis.

2.2. Measurements related to the PLC bands

Full thickness, flat tensile specimens, with a gauge length of 80 mm and 20 mm wide, were cut from the sheet and tested under displacement control at three different actuator speeds: 0.05, 0.5 and 5 mm/s, corresponding to mean strain rates of 0.0004, 0.004 and 0.04 s^{-1}.

In order to not interfere with the infrared thermography and optical extensometry techniques, no electrical extensometers were applied on the specimen in most tests and the total axial strain was obtained from the actuator displacement, after a calibration was performed with a clip-on axial extensometer mounted on nominally equal samples.

The thermographic tests were performed with an infrared camera sensitive to the 8-14 μm wavelength range. A black coating is generally applied on thermographic specimens to obtain a homogeneous high thermal emissivity [17]; in the present case, a graphite lubricant (applied by spraying) was used for this purpose, to avoid the exfoliation that other coatings showed with large tensile strains. The thermal images were recorded at a frequency of 29.4 or 3.0 Hz for tensile tests

performed at strain rates of 0.0004 or 0.04 s^{-1}, respectively. The spatial resolution on the specimen surface was about 0.4 mm (with small variations due to the camera distance). Because of the uncertainty regarding the thermal emissivity and the view factor, the temperature values calculated from the recorded IR intensity are considered approximate.

The thermographic data were examined as follows.

First, the nucleation times and locations of the A and C bands and the propagation directions of the A bands were identified in the thermal (i.e., infrared) video recording, and the inclination of the C bands were measured in the relevant thermal images (no B bands were observed).

Moreover, by examining the time - temperature plot of four measurement points lying on the specimen axis, which exhibit sharp temperature steps when a band passes through them, both the local temperature increases associated with the A bands transits and the propagation speed of the same type A bands could be determined. In particular, the propagation speed of the A bands were first determined in the camera reference system, measuring the band transit times across two successive measurement points.

The latter band propagation speeds were then reported into the reference system of the least deformed part of the specimen, i.e. the part not yet reached by the propagating band itself, by subtracting the actuator speed when appropriate; this correction is necessary because bands could be moving either towards the specimen's fixed end, connected to the machine frame, or toward the specimen's moving end, connected to the actuator, whereas the thermal camera, and hence the four measurement points, were always fixed in respect to the machine frame.

Finally, the strain occurring in a band was calculated from its propagation speed, by hypothesizing that, when the band is active, the deformation occurs only in the band itself, and by using the reference system in which the band is still and the material enters into the band with a lower speed V_{in} and exits from the band with an higher speed V_{out}. With these hypotheses, the material incoming speed, V_{in}, is equal to the above defined band propagation speed; the speed difference, V_{out} - V_{in}, is equal to the known actuator speed, V_a; and the band material balance is: $S_{in}V_{in} = S_{out}V_{out}$, where S_{in}

and S_{out} are the cross sections of the incoming and outgoing material. With this, the strain that occurs inside the band can be calculated as follows: $\varepsilon_b = S_{in}/S_{out} - 1 = (V_{out}-V_{in})/V_{in} = V_a/V_{in}$.

The optical strain measurements were performed by digital image correlation. A high-contrast stochastic pattern was applied on one plane face of each tensile specimen by spraying first a continuous layer of a black graphitic lubricant and then a discontinues pattern of white paint spots; this coating persisted until the end of the tensile test. During the tensile test, a series of images of the prepared specimen face were acquired with a digital camera at an acquisition frequency of 0.3, 3 and 10 Hz for tests performed with mean strain rates of 0.0004, 0.004 and 0.04 s^{-1}, respectively. The specimen planar displacement field was eventually calculated with a dedicated software by comparing the positions of recognizable features of the surface pattern among successive images.

The planar displacements were first calculated in a set of points which, at the start of the test, formed a square or rectangular lattice in the examined plane, with a cell size on the order of 1.5 mm (with small variations among different tests). The desired displacement, strain and strain rate values were then calculated in any desired surface point by means of suitable interpolations and derivations. In particular, both strain animations, produced by mounting several frames, each showing the two-dimensional color-coded map of the major strain at a given time during the tensile test, and plots of the major strain and strain rate as a function of the axial position along three measurement lines parallel to the specimen axis at successive tests times, were examined.

The extensometric data was examined as follows. First, the nucleation times and locations and the propagation directions of the type A bands were identified by observing the strain animations (neither B bands, nor individual C bands were detected). Furthermore, the data pertaining to the measurement lines were used as follows. First, the true strain occurring inside the A bands was calculated as the difference between the axial (i.e., major) true strain values of the most-deformed material, already crossed by the examined A band, and of the least-deformed material, not yet reached by the same A band. Moreover, the successive positions of a given A band along a measurement line were determined as the points exhibiting the peak strain rate in successive

measurement times, allowing to calculate the propagation speed of the same A band in the camera reference system; this speed was then reported in the reference system of the least deformed material, as explained above.

3. RESULTS AND DISCUSSION

The A bands were detected and measured by both of the above mentioned techniques, whereas the C bands were detected individually only by infrared thermography. These latter observations reveal that the C bands often occur in sequences where each band is immediately ahead of the previous one, in the same tensile axis direction, and most often with the same inclination, in agreement with previous optical examinations of polished specimens [12]. The optical extensometry generally does not detect individual C bands, but it reveals the overall strain effect of a series of successive C bands. In a strain animation, a single A band appears as a sharp moving edge with a constant inclination, whereas a sequence of C bands appears as a blunt moving edge whose inclination can change several times between the two opposite variants foreseen by the strain localization theories; hence the two phenomena can generally be distinguished.

Fig. 2a shows a major-strain map determined by optical extensometry during a tensile test performed at a strain rate of 0.004 s^{-1}, for an A band moving from left to right. In Fig. 2b the same map is superimposed onto the sample image. In addition, in Fig. 2c, the strain is plotted as a function of position along the three measurement lines parallel to the sample axis, which are sketched in Fig. 2a. Both the maps and curves reveal a remarkable strain step, due to the A band.

In Fig. 3, pertaining to the same test, the major strain measured by optical extensometry on the measurement line corresponding to the sample axis is plotted at successive times starting from the nucleation of an A band. The curves relating to different instants of time show a strain step in different positions, from right to left, while the band moves along the tensile axis. By comparing successive times, it is noted that the strain is almost constant everywhere, except in the portion of the sample crossed by the band; therefore, within the uncertainty limits of the present strain

measurement method, it is concluded that the whole deformation of the sample is localized in the band. Moreover, the strain increment caused by the band, i.e. the height of the strain step, is almost constant during the transit of the band along the whole specimen length.

By observing the strain animations of the tensile tests carried out at strain rates of 0.0004, 0.004 and 0.04 s^{-1}, it was determined that only one A band was active at any time, and that most new A bands initiated close to the specimen mid-length while the preceding one reached one end of the specimen, even if a band travelled along the whole sample length in some cases as illustrated in Fig. 3.

In Fig. 4, the nucleation times of the A bands, as observed with the thermal camera on the surface of a sample tested at 0.0004 s^{-1} strain rate, are compared with the stress-time curve of the same specimen. This type of examination was performed on many specimens and revealed that the nucleation times of the A bands always corresponded to a stress peak.

The above defined propagation speeds of the A bands (in the reference system of the least deformed part of the specimen) and the strain occurring inside the same bands were determined in two different tensile tests performed at a strain rate of 0.0004 s^{-1}, using optical extensometry in one test and infrared thermography in the other one. About ten consecutive bands were studied in detail in each test, with the above explained methods. The results are shown in Fig. 5 as a function of the overall engineering strain of the specimen at the time of nucleation of each band. Moreover, Fig. 6 shows the temperature increase caused by the same bands in the sample analyzed using thermography.

The propagation speed of the A bands gradually decreases during the test, while the strain caused by the same bands increases. This inverse relation between the propagation speed and the associated strain of the A bands was implicitly assumed in the above described thermographic data reduction method, but it has been confirmed by independent measurement of the two quantities performed by the extensometric method. Finally, the temperature step associated with the A band transits increases during the test, which is consistent with increasing band strain.

In the stress-strain curves, the type C bands induce serrations corresponding to sudden stress falls followed by linear reloading. The infrared thermography recording clearly showed that each stress decrease corresponded to a single band (Fig. 7a). Fig. 7b shows four successive type C bands, belonging to the same sequence, with one inclination change between the 3rd and the 4th band. Between two successive C bands it was always possible to record a thermal image in which the thermal trace of the first band is fading, presumably due to the heat diffusion after the end of the localized deformation, while the second band has not yet appeared; this fact confirms that each band is separated in time from the previous one. The inclination of the C bands with respect to the sample axis is about 53.6°, and the bands belonging to the same sequence appear at regular space and time intervals, approximately equal to 2 mm and 2.5 s, respectively, in the test performed at a strain rate of 0.0004 s^{-1}. The above inclination confirms previous findings by Spretnak [18].

The overall strain effect of some C bands sequences, detected by optical extensometry in the 0.0004 s^{-1} strain rate test, was also examined as if it was due to a single A band (neglecting the inclination changes). This allowed to conclude that the “propagation speed” and “associated strain” of the C band sequences were broadly consistent with the trend of the preceding A bands.

4. CONCLUSIONS

The 22% Mn, 0.5% C, austenitic, fine-grained steel studied at room temperature shows a remarkable combination of strength and ductility (1090 - 1180 MPa ultimate tensile strength and 55 - 65 % total elongation), due to the intrinsic ductility of the austenite and the formation of mechanical twins [7]. Contrary to other austenitic steels, this material does not exhibit strain induced phase transformations, probably due to a relatively high stacking fault energy [7,12,19].

The tensile curves obtained at different strain rates show an inverse relation between the flow stress and strain rate, a condition that is known to promote inhomogeneous plastic strain [15]. In fact, during the tensile tests the Portevin-Le Chatelier strain localization phenomena were observed, consisting of both A bands (which move along the sample axis) and C bands (which do not). With

increasing strain rate, the PLC phenomena start at higher strain values, and finally disappear at a strain rate between 0.04 and 0.3 s^{-1}.

Optical extensometry confirmed that when an A band is active the plastic strain is totally localized in the band itself, as it was previously hypothesized [12].

Moreover, both optical extensometry and infrared thermography showed that the nucleation of an A band is contemporaneous to a stress peak on the stress-strain curve, whose formation can be explained as follows: normally the local strain rate in an active A band is higher than the average strain rate of the whole sample, therefore the stress is lower than that necessary for homogeneous deformation, and rises to the latter value only when the band reaches the head of the specimen and disappears, forming the stress peak; thereafter, a new band appears and the stress returns to its previous lower value.

Consistent results were obtained for the propagation speed and associated true strain of the A bands by both infrared thermography and optical extensometry.

With increasing total strain, the propagation rate of the A bands decreases, while the true strain and the local temperature rise due to each band increases. The latter thermal effect is certainly caused by the increase of both the band strain and the steel flow stress (due to strain hardening).

The C bands generally occur in sequences, each being immediately ahead of the previous one, in the same tensile axis direction, and most often with the same inclination, which is consistent with previous observations on different materials [20]. Optical extensometry reveals the overall effect of the C bands sequences, while infrared thermography detects each C band individually. In particular, it was verified that each serration (sudden stress drop) of the stress-strain curve corresponds to the activation of a C band.

The present results and interpretation regarding the occurrence of type A PLC bands during room temperature tensile tests are in overall agreement with recent observations in similar high-Mn TWIP steels [11,13,14], even if the occurrence of C bands was not reported in those studies; this

discrepancy may be due either to the different observation methods used, or to small differences in the steel composition and microstructure.

REFERENCES

1 D. Cornette, P. Cugy, A. Hildenbrand, M. Bouzekri, G. Lovato, *Revue de Metallurgie*, 12 (2005), 905-918.

2 O. Grassel, G. Frommeyer, *Materials Science and Technology*, 14 (1998), 1213-1217.

3 O. Grassel, L. Kruger, G. Frommeyer, L. W. Meyer, *International Journal of Plasticity*, 16 (2000), 1391-1409.

4 P. Yang, Q. Xie, L. Meng, H. Ding, Z. Tang, *Scripta Materialia*, 55 (2006), 629-631.

5 S. Vercammen, B. Blanpain, B.C. De Cooman, P. Wollants, *Acta Materialia*, 52 (2004), 2005-2012.

6 O. Bouaziz, N. Guelton, *Materials Science and Engineering A*, 319-321 (2001), 246-249.

7 S. Allain, J.P. Chateau, O. Bouaziz, *Material Science and Engineering A*, 387-389 (2004), 143-147.

8 S. Allain, J.P. Chateau, O. Bouaziz, *Steel Research*, 73 (2002) 299-302.

9 G. Frommeyer, U. Brux, P. Neumann, *ISIJ International*, 43 (2003) 438-446.

10 L. Chen, H.S. Kim, S.K. Kim, B.C. De Cooman, *ISIJ International*, 47 (2007), 1804-1812.

11 P.D. Zavattieri, V. Savic, L.G. Hector, J.R. Fekete, W. Tong, Y. Xuan, *International Journal of Plasticity*, 25 (2009), 2298-2330.

12 G. Scavino, F. D'Aiuto, P. Matteis, P. Russo Spena, D. Firrao, *Metallurgical Materials Transactions A*, 41 (2010), 1493-1501.

13 J.K. Kim, L. Chen, H.S. Kim, S.K. Kim, G.S. Kim, Y. Estrin, B.C. De Cooman, *Steel Research International*, 80 (2009), 493-498.

14 T.A. Lebedkina, M.A. Lebyodkin, J.P. Chateau, A. Jacques S. Allain, *Material Science and*

Engineering A, 519 (2009) 147-154.

15 E. Rizzi, P. Hahner, *International Journal of Plasticity*, 20 (2004), 121-165.

16 S. Allain, P. Cugy, C. Scott, J.P. Chateau, A. Rusinek, A. Deschamps, *International Journal of Materials Research*, 99 (2008), 734-738.

17 F. Curà, G. Curti, R. Sesana, *International Journal of Fatigue*, 27 (2005), 453-459.

18 C.A. Griffis, J.W. Spretnak, *Transactions of the Iron and Steel Institute of Japan*, 9 (1969), 272.

19 L. Remy, A. Pineau, *Material Science and Engineering*, 28 (1977) 99-107.

20 L.J. Cuddy, W.C. Leslie, *Acta Metallurgica*, 20 (1972), 1157-116.

FIGURES

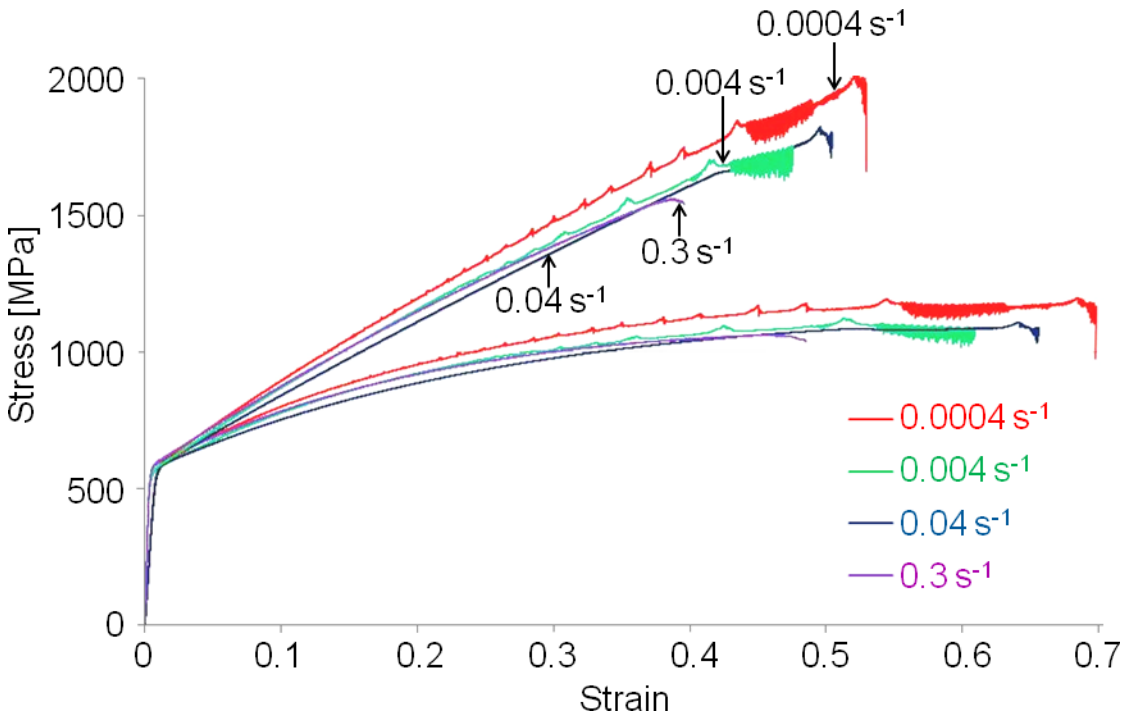

Fig. 1: Typical engineering (a) and true (b) stress-strain curves of the TWIP steel, as a function of strain rate. [12]

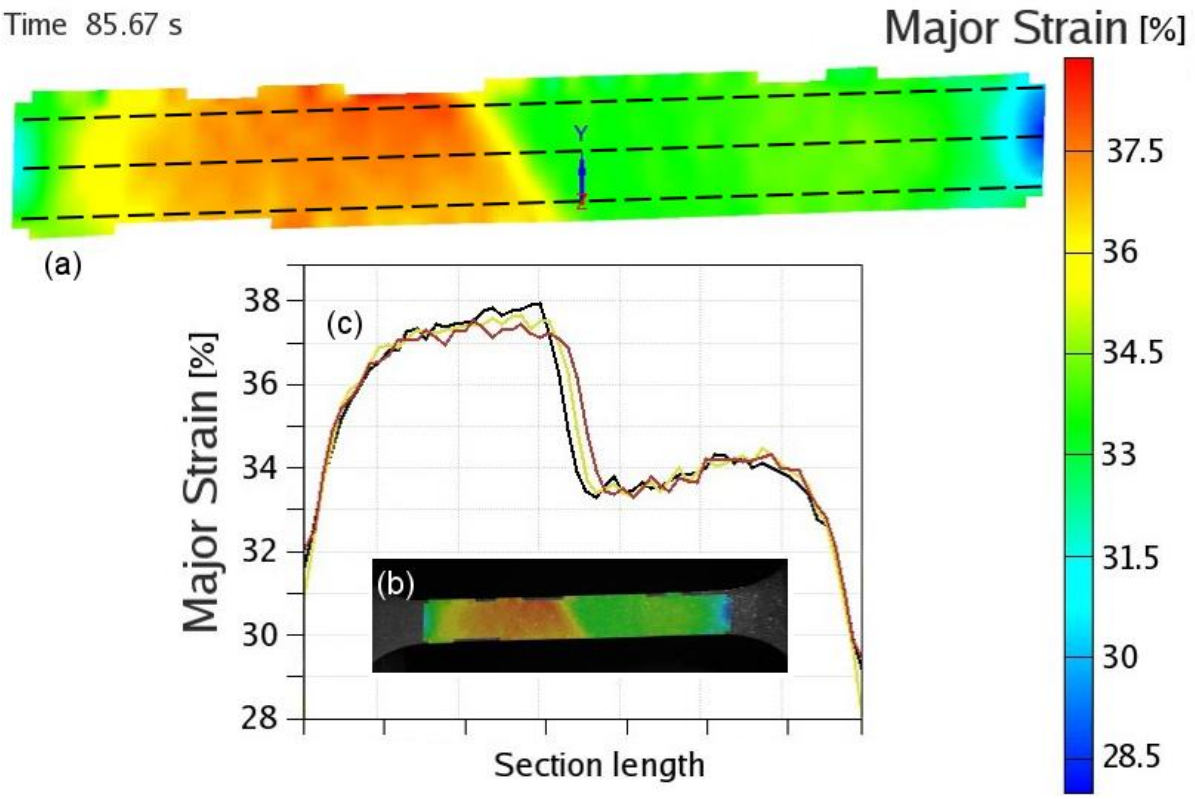

Fig. 2: Tensile test at a strain rate of 0.004 s^{-1}. Major strain measured by optical extensometry: color-coded map of the whole sample (a), same map superimposed to the sample image (b), and plots pertaining to the three shaded segments (c). In color in the on-line version.

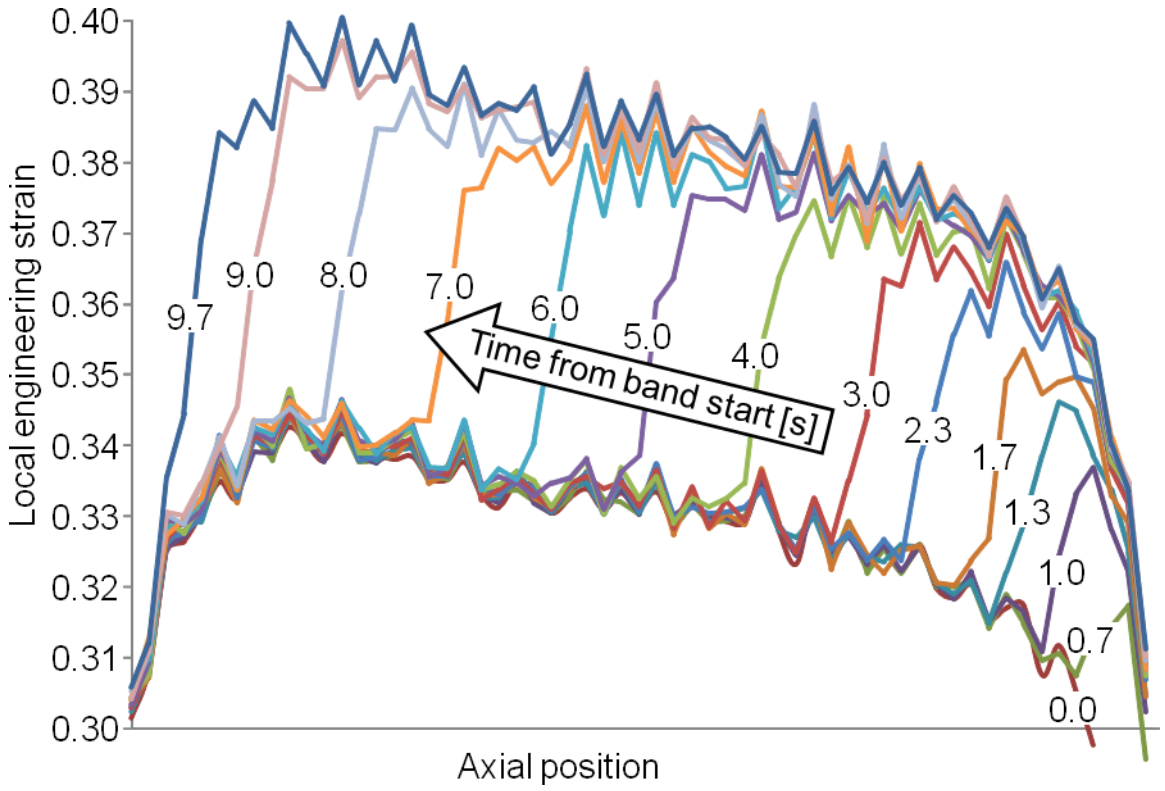

Fig. 3: Tensile test at a strain rate of 0.004 s^{-1}. Pointwise strain along the specimen axis, as determined by optical extensometry, at successive times, while an A band is active.

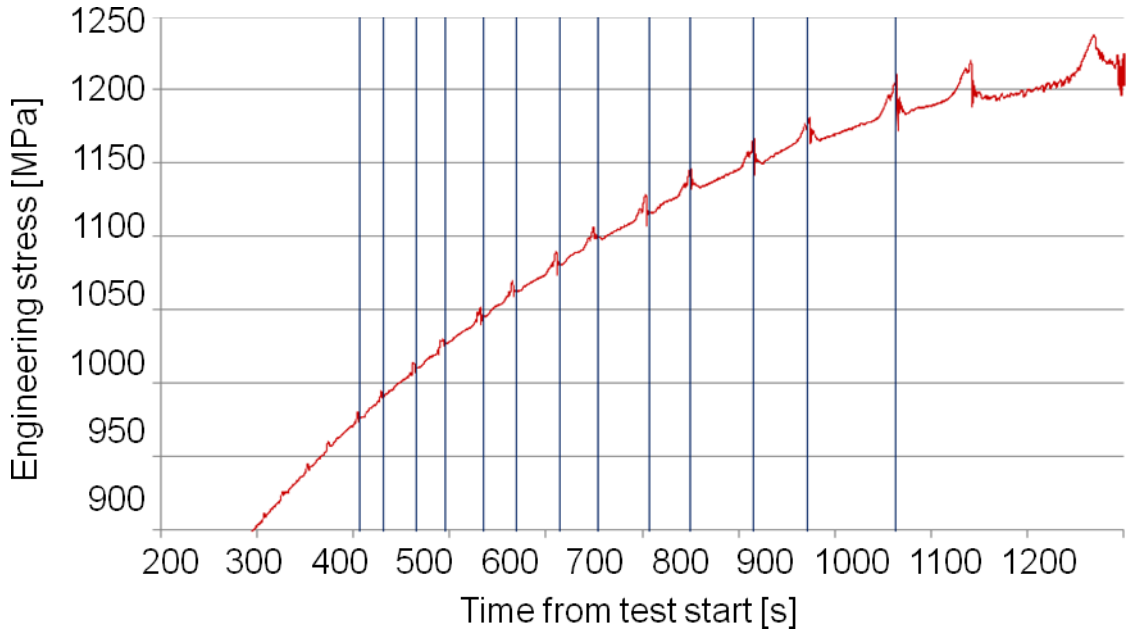

Fig. 4: Tensile test at a strain rate of 0.0004 s^{-1}. Engineering stress as a function of time (curve), compared with the A bands nucleation times detected by infrared thermography (vertical lines).

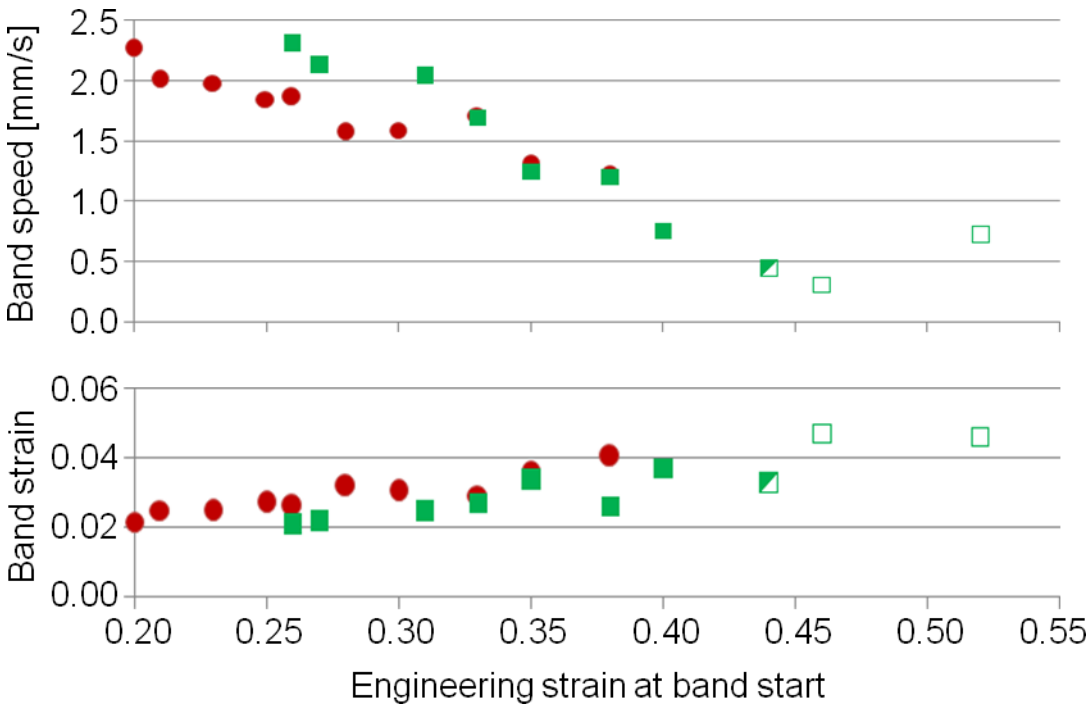

Fig.5: Tensile tests at a strain rate of 0.0004 s^{-1}. Propagation speed and associated true strain of A bands, evaluated by infrared thermography (circles) or by optical extensometry (filled squares), as a function of overall engineering strain at the band nucleation time, and same quantities evaluated by optical extensometry for sequences of C bands (empty squares) and for one uncertain feature being either an A band or a sequence of C bands (half-filled squares).

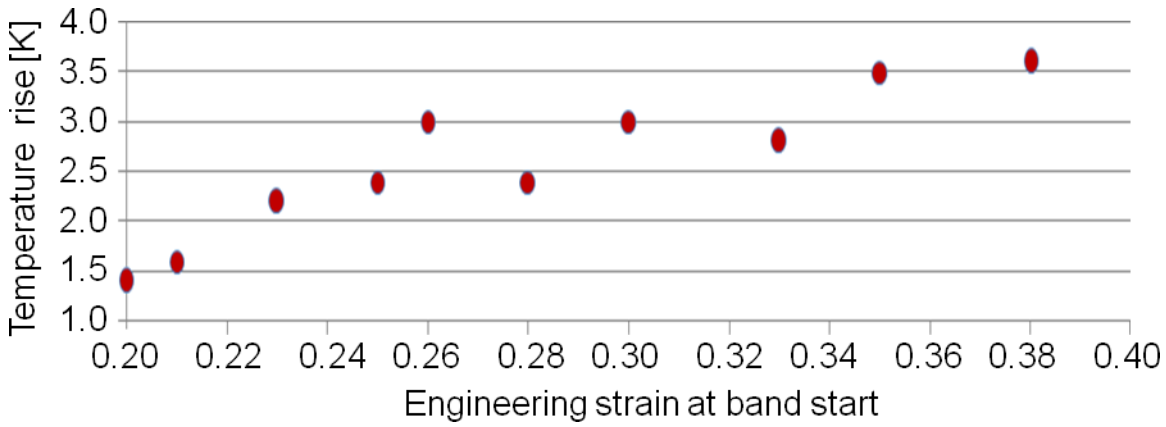

Fig. 6: Tensile tests at a strain rate of 0.0004 s^{-1}. Local temperature rise due to A bands, evaluated by infrared thermography, as a function of overall engineering strain at the band nucleation time.

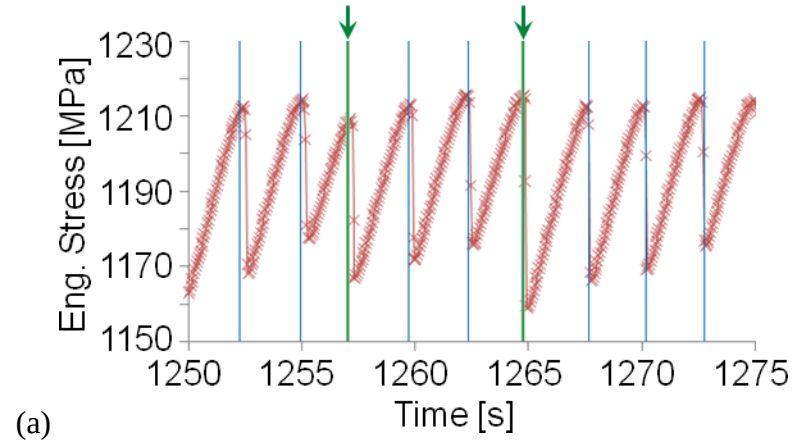

(a)

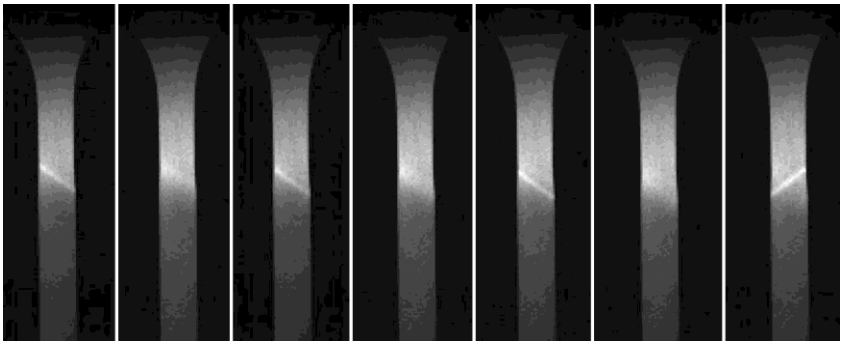

(b)

Fig. 7: Tensile tests at a strain rate of 0.0004 s^{-1}. Infrared thermography. Engineering stress - time curve, activation times of C bands (vertical lines) and of C bands with inclination changes (vertical lines indicated by arrows) (a). Sequence of thermal images showing four C bands with one inclination change (b).

TABLES

Speed	**Strain Rate**	**YS**	**UTS**	**$d\sigma/d\varepsilon_p$**	**A_t**
mm/s	s^{-1}	MPa	MPa	MPa	%
0.05	0.0004	551	1178	2870	61
0.5	0.004	541	1118	2737	61
5	0.04	548	1093	2695	58
39	0.3	557	1063	2620	49

Tab. I. Mean tensile properties of the TWIP steel, as a function of strain rate (YS: yield stress, UTS: ultimate tensile strength, $d\sigma/d\varepsilon_p$: true strain-hardening slope, A_t: total elongation-to-fracture) [12].